Fabrication and characterization of nano-ZrO_2 dispersed W-based alloys by mechanical alloying and conventional sintering

A. Patra*, S. K. Karak, R.Saxena

Department of Metalurgical and Materials Engineering, National Institute of Technology, Rourkela 769008, India

Abstract

Nanostructured tungsten (W) based alloy with the nominal compositions of 1.0 wt. % nano-ZrO_2 dispersed $W_{79}Ni_{10}Mo_{10}$ (in wt. %) was synthesized by mechanical alloying followed by compaction at 1GPa pressure for 5 mins and conventional sintering at 1500°C for 2 h in Argon atmosphere. The microstructure and evolution of phases during milling and consolidated products was investigated by X-ray diffraction (XRD), scanning electron microscopy (SEM), High resolution transmission electron microscopy (HRTEM) and Energy dispersive spectroscopy (EDS). Minimum crystallite size of 28.6 nm and maximum lattice strain and dislocation density of 0.29% and 12.67 ($10^{16}/m^2$) respectively was achieved in $W_{79}Ni_{10}Mo_{10}(ZrO_2)_1$ alloy at 20 h of milling. The lattice parameter of W in $W_{79}Ni_{10}Mo_{10}(ZrO_2)_1$ alloy expanded upto 0.02% at 5 h of milling and contracted upto 0.20% at 20 h of milling. The hardness of the sintered alloy was 4.92 GPa with appreciable wear resistance.

Keywords: W based alloy; Mechanical alloying; Oxide dispersion; Hardness; Wear

1. Introduction

Tungsten is a potential material for electrical, electronic, nuclear reactor and space vehicle applications due to high melting point (3410°C), excellent mechanical strength at elevated temperature, highest density (19.3 g/ml), hardness of 9.8 GPa, high tensile elastic modulus (411 GPa at 20°C) [1, 2].

Amorphous and nanocrystalline tungsten alloys have gained significant attention in recent years due increasing demand for higher and better mechanical properties. Nanocrystalline materials possess extremely high hardness and yield strength. Mechanical alloying is a convenient solid state synthesis alternative to rapid quenching [3, 4] to improve the mechanical properties of tungsten alloys by microstructural refinement. Recent literature reports that consolidation of conventional microcrystalline W powder is difficult [5]. Gurwell [6] and Uray [7] has reported that consolidation of W based alloys require temperature more than 2700°C. Recent investigation reveals that the pure W can be sintered at ~1800°C temperature as compared to conventional sintering temperature of 2700°C by synthesis of nanostructured W-powder before sintering [8]. Hahn *et al.* have also reported a similar behavior of reduced sintering temperature with decrease in the crystallite size of TiO_2 [9]. At high temperature formation of volatile oxide on the surface of tungsten limits its application. Formation of protective coating on tungsten surface is therefore essential for its high temperature application. Addition of alloy in pure tungsten improves the possibility of high temperature applications [10]. Recent literature suggest that transition metal addition modifies the dislocation core from symmetric to asymmetric which results in reduction of the Peierls stress (stress required for a dislocation to move) and improvement of the ductility of a material [11]. Same behavior is expected to be achieved by addition of nickel. Nickel facilitates sintering by formation of liquid phase due to lower melting point (1455°C) as compared to the present sintering temperature (1500°C). Addition of Mo provides strength, hardness with appreciable ductility to W base alloys [12].

The recrystallization and grain growth of W matrix for high temperature applications is hindered by the presence of fine and uniform oxide particles dispersion at the grain boundary of tungsten. The high temperature strength and creep resistance of the matrix improves by the grain boundary pinning and inhibiting the grain boundary sliding at high temperature by the dispersed oxide [13]. The fine dispersed oxides are thermodynamically stable fine and inert with the matrix phase. Dispersion of thoria (ThO_2) in W matrix leads to increase the recrystallization

temperature and results in improvement of hot strength and creep resistance as compared to W alloys [13]. Development of thoria free oxide dispersion strengthened (ODS) tungsten materials is necessary due to radioactive radiation effect from thoria.

Recent literature reports the synthesis and characterization of several tungsten based ODS alloys [14-16], however no reports are available on W-Ni-Mo-ZrO_2 alloy till date. Present research work aims at reduction in the sintering temperature of W-based alloys by fabrication of nanostructured powders by mechanical alloying (MA) before sintering as well as to investigate the microstructure, physical and mechanical properties of the fabricated W-Ni-Mo-ZrO_2 alloy.

2. Experimental

A high energy planetary ball mill (Fritsch, P5) was used for mechanical alloying of elemental powders of W, Ni, Mo, ZrO_2 (purity 99.5%, Sigma Aldrich) with initial particle of 100-150 μm (for W, Ni, Mo) and <50 nm (for ZrO_2). Toluene atmosphere was used to prevent excessive welding and chrome steel was used as grinding medium. The mill speed and ball to powder weight ratio was maintained as 300 r.p.m and 10:1 respectively. Milled samples were taken out after 1, 5, 10, 20 h for characterization purpose.

The X-ray diffraction pattern (XRD) of the mechanically alloyed powders at different stages of milling was investigated by high resolution X- ray diffractometer (RIGAKU Japan, Ultima IV) using Cu-k_α radiation (λ=1.541874 Å). The record was matched with the JCPDS data bank to track the evolution of phases during mechanical alloying [17]. The crystal size and lattice strain was evaluated by determining the peak position and broadening of peak from the X- ray diffraction pattern [18]. The lattice parameter was calculated from the X-ray diffraction pattern by using precise lattice parameter calculation method [18]. The dislocation density of the milled powders has been evaluated as below:

$$\rho_d = 2\sqrt{3}\frac{(\varepsilon^2)^{1/2}}{D \text{ X } b} \qquad (1)$$

Where, b is the burgers vector of dislocations, b = (a√3)/2 for the bcc structure, a= cell parameter = lattice parameter, D = crystallite size, ε = lattice strain, [19].

The morphology of milled powders was determined by scanning electron microscope (JEOL, JSM-6084LV).

The 20 h milled powder contained in the test tube was dissolved in acetone and vigorously stirred in ultrasonic stirrer. The powder was placed on the carbon grid before HRTEM study. A high resolution transmission electron microscope (JEOL, JEM 2100) with accelerating voltage of 200 KV, and lattice resolution of 0.14 nm was employed to detect the size of the crystal in mechanically alloyed powders by bright field imaging technique. Selected area diffraction (SAD) pattern was used to identify the crystal structure.

The 20 h milled powders were subjected to compaction in a uniaxial press at 1 GPa pressure for 5 minutes. Sintering of the compacted pellets was carried out in a tunnel type sintering furnace at 1500°C for 2 hours by purging argon into the furnace at a rate of 100 ml/min. The density of the sintered product was calculated by Archimedes' principle. The sinterability was evaluated from the percentage ratio of density of the sintered sample to theoretical density of the sintered sample. X-ray diffraction and scanning electron microscopy were used to investigate the phase evolution and microstructure of the sintered product. The dispersed particles in sintered alloy were observed under high resolution transmission electron microscope (JEOL, JEM 2100). The bulk sample was thinned by polisher and ion milling before HRTEM study. Wear test was performed by a ball on plate wear tester (DUCOM, TR-208-M1) with 20 N and 30 N load, time and sliding speed and track diameter of 10 mins, 25 r.p.m, 4 mm respectively. Wear depth was recorded with sliding distance traversed by the indenter on the sintered sample. Microhardness of the sintered product was determined by a Microhardness tester (LECO, LM248AT) with 50-g load and 10 sec dwell time.

3. Results and discussion

3.1. Characterization of milled powder

Figure 1 shows the evolution of phases of the milled powder with increase in milling time from 0 to 20 h as determined by XRD analysis. It is evident from Figure 1 that the broadening of the XRD peaks increases whereas intensity decreases due to plastic strain buildup and refinement of crystallite size. Formation of solid solution is evident at 20 h of milling and no sharp peak of W, Ni, Mo, ZrO_2 were detected. The crystallite size of W reduced to 28 nm whereas lattice strain

increased to 0.29% with increase in milling time from 0 h to 20 h as measured by Scherrer equation (figure 2(a)). The considerable crystallite size reduction of W was due to high surface energy associated with ZrO_2 nanoparticles, which induces higher energy and plastic deformation into W lattice. Figure 2(b) displays the variation of particle size (measured from multi point measurement utility of SEM) at different milling time. The average particle diameter decreased to 11.13 μm with increase in milling time from 0 to 20 h.

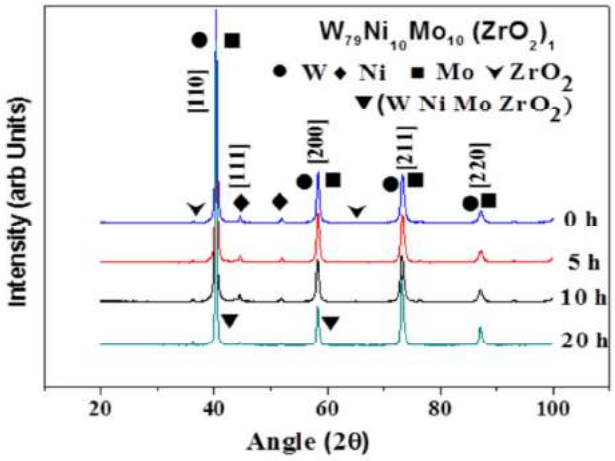

Fig. 1. XRD pattern of milled powder at different times of milling.

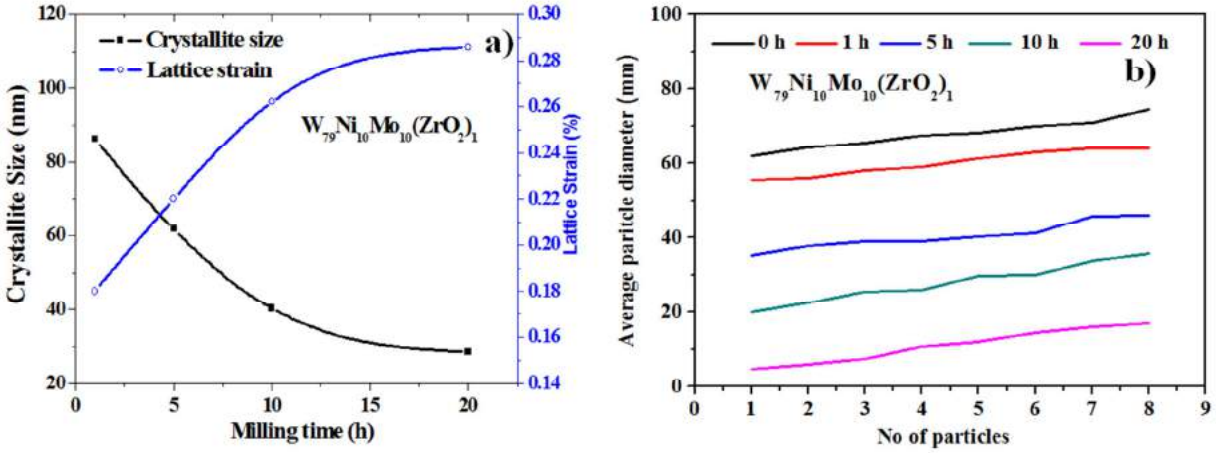

Fig. 2. Variation of a) crystallite size and lattice strain b) average particle size with milling time.

Figure 3(a) shows the variation of dislocation density with increase in milling time. The dislocation density increases sharply upto 10 h of milling, however the rate of increase of dislocation density decreases beyond 10 to 20 h of milling. The initial sharp increase in

dislocation density is attributed to substantial crystallite size reduction from 0 to 10 h of milling. The decrease in the rate of dislocation density beyond 10 h of milling is due to formation of solid solution which dominates over crystallite size reduction. Figure 3(b) illustrates the variation of lattice parameter of W with increase in milling time. The atomic radius of W (0.193 nm) is larger than Ni (0.149 nm) and Mo (0.190 nm). The initial marginal expansion (0.02%) of W lattice is due to exertion of negative hydrostatic pressure by formation of nano-crystallites. Similar expansion in Nb lattice was reported by Pabi *et al.* during milling of pure Nb [20]. The lattice parameter of W displayed sharp contraction upto 0.20% beyond 10 to 20 h of milling due to formation of substitutional solid solution by Ni and Mo with W matrix.

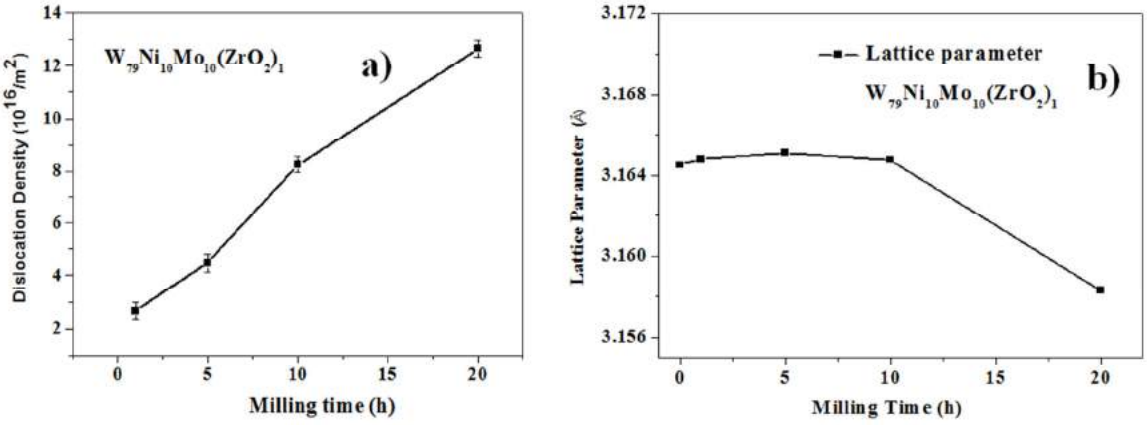

Fig. 3. Variation of a) dislocation density b) Lattice parameter with milling time.

Figure 4 displays the SEM micrograph which illustrates the variation in particle size and morphology at different milling time. The irregular shape of initial powders transformed to uniform shape and homogeneous size distribution with continuous refinement of particle at 20 h of milling. The particles were subjected to extensive strain hardening and fractured with increase in milling time. No substantial agglomeration of powder particles was evident due to proper presence of toluene during milling.

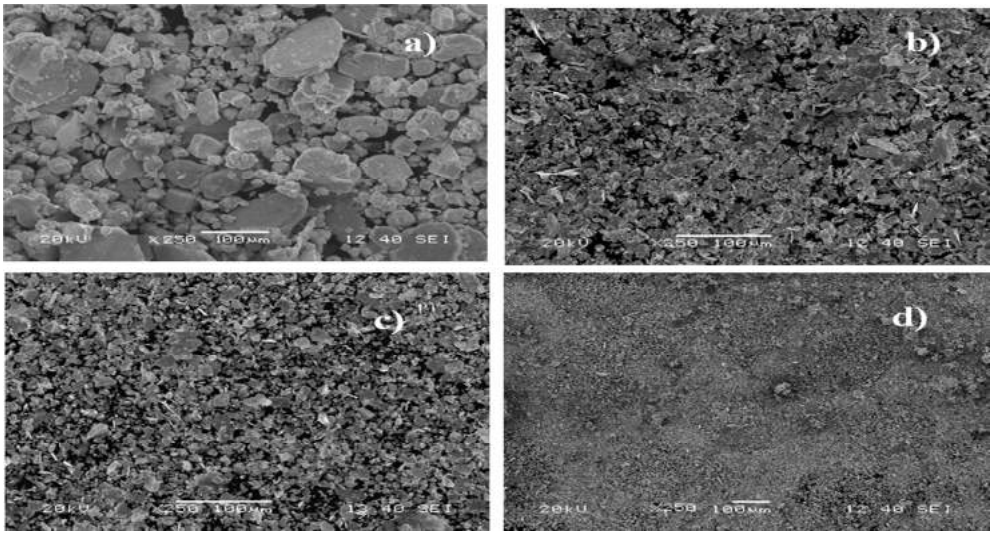

Fig. 4. SEM images of powder morphology at different milling times: (a) 0 h, (b) 5 h, (c) 10 h, and (d) 20 h.

Figure 5 (a) shows the bright field TEM image with selected area diffraction (SAD) pattern (figure 5(b)). The average crystallite size of the 20 h milled powder is in the range of 20-30 nm. The observed crystallites size from TEM image was in well agreement with the crystallites size derived from XRD analysis (figure 2(a)). Formation of fine polycrystallites was evident from the continuous rings of SAD pattern. The interplaner spacing (*d)* of BCC-W for the planes evaluated after indexing of SAD pattern was measured as 0.22 nm for (110), 0.15 nm for (200), and 0.09 nm for (222) respectively. XRD pattern (figure 1) confirmed the *d* spacing values of BCC-W as measured from SAD pattern.

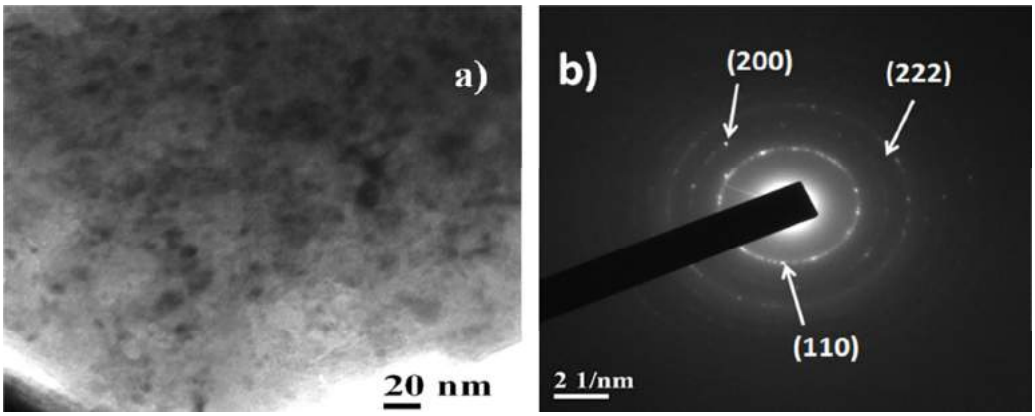

Fig. 5. (a) Bright field and corresponding (b) SAD pattern for 20 h milled powder.

3.2. Characterization of sintered product

Density of the sintered alloy was calculated by Archimedes' principle [21] as below:

$$\rho_s = \frac{W_a}{(W_{sat} - W_{susp})} X \rho_w \frac{gm}{cm^3} \quad (2)$$

$\mathbf{W_a}$ is weight of the sintered sample in air. $\mathbf{W_{sat}}$ is the weight of the sample with all the open porosity saturated with water, $\mathbf{W_{susp}}$ is the weight suspended in water. $\boldsymbol{\rho_w}$ is the density of water. The sinterability (sintered density: theoretical density) of the alloy milled for 20 h and sintered at 1500°C for 2 h was recorded 90.8% by pressing at 1 GPa pressure for 5 mins.

Figure 6 shows the XRD pattern of the alloy sintered at 1500°C for 2 h. Formation of hard, brittle MoNi intermetallic and presence of ZrO_2 is evident from the XRD pattern. The strength of the W matrix could be enhanced by the MoNi intermetallic phase and ZrO_2 by dispersion strengthening mechanism [22]. Lin *et al.* also reported formation of similar MoNi intermetallic phase in W base alloy [23].

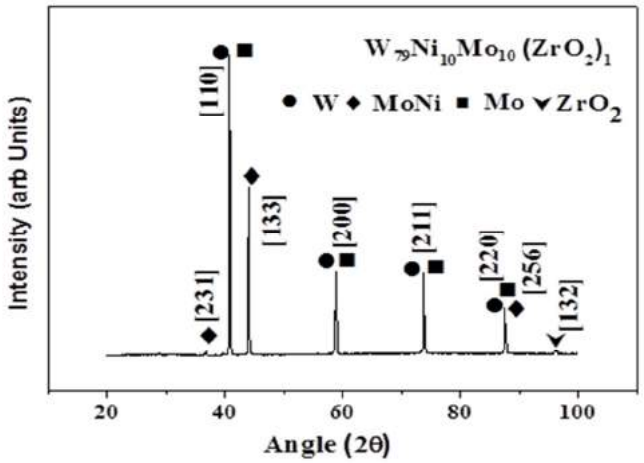

Fig. 6. XRD pattern of sintered alloy milled for 20 h and sintered at 1500°C for 2 h.

Figure 7 displays the SEM micrograph of the sintered alloy. Presence of MoNi intermetallic (dark phase) is evident aside of W grains (bright phase) from the micrograph. The formation of MoNi intermetallic was attributed to the lower melting point of Ni (1455°C) as compared to the sintering temperature selected for present study (1500°C). The phases identified from SEM

micrograph agreed with the identified phases from the XRD pattern. The grain size of W as measured from SEM micrograph was ~12 μm. Marginal porosity is also evident from the SEM micrograph.

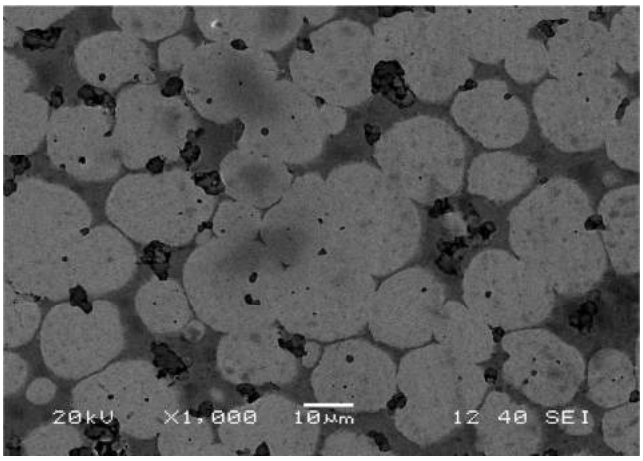

Fig. 7. SEM micrograph of the sintered alloy at 1500°C.

Figure 8 displays the high resolution TEM (HRTEM) image of the sintered alloy. Presence of ZrO_2 nanoparticles at the grain boundary is evident from TEM image. Recent literatures report that the grain boundary pinning effect induced by the nanoparticles and strong dislocation and nanoparticles interaction is responsible for enhancement of the strength and hardness of the matrix [22, 24]. The inset image shows the energy dispersive spectrometry (EDS) which confirms the presence of ZrO_2 nanoparticles.

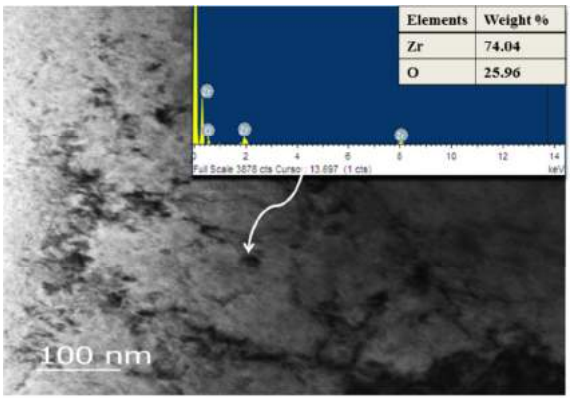

Fig. 8. Bright Field HRTEM image of alloy sintered at 1500°C for 2 h, Dispersed ZrO_2 particles at the grain boundary, inset displays the EDS pattern of the dispersed ZrO_2 particle.

Figure 9 shows the variation of hardness with 10 different indentations along of the cross section of the sintered alloy. The average hardness was measured as 4.92 GPa. The hardness is 2-2.5 times higher than recent reported hardness value of W base alloy [23, 25]. The enhancement in the hardness value can be attributed to the dispersion strengthening effect of ZrO_2 nano particles, increase in Ni wt. % as compared to recent study [25] which facilitates more effective pore filling by liquid phase sintering.

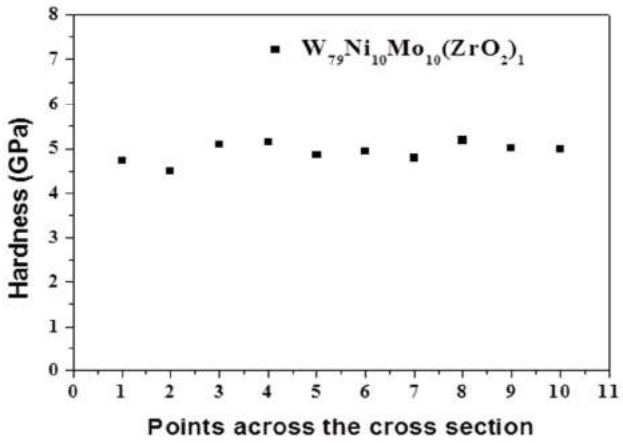

Fig. 9. Variation of Hardness of alloy sintered at 1500°C for 2 h.

Figure 10 shows the variation of wear depth with sliding distance at various load (20 N and 30 N). It is evident from figure 10 that the wear depth or wear loss increases with increase in test load. Figure 11 (a) and (b) show the SEM micrograph of wear track at 20 N and 30 N loads respectively. SEM micrograph of wear track reveals that the track width increases with increase in the load. The wear rate measured by archard equation [26] as evident from table 1 also increases with increasing load. The hard intermetallic phases and ZrO_2 particles are removed from the matrix during abrasive wear phenomenon. Recent reports suggest that considerable removal of hard particles could enhance the wear by three body motion process [24, 27]. The increase in the wear at 30 N load as compared to 20 N is due to presence of removed hard particles on the wear track which results in enhanced abrasion and higher wear loss.

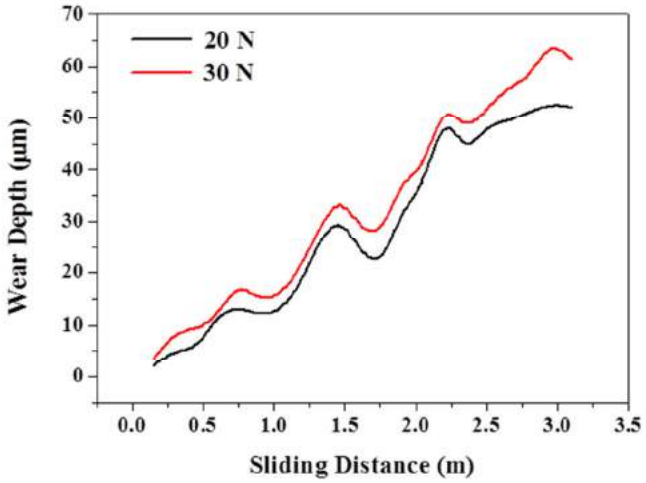

Fig. 10. Variation of wear depth with sliding distance for the sintered alloy.

Table 1. Wear rate at different load

Applied Load (N)	Maximum Wear depth (µm)	Maximum sliding distance (m)	Track Diameter (m)	Wear rate 10^{-15} (m^{3}/N m)
20	52.44	3.10	0.004	2.68
30	63.36	3.10	0.004	2.76

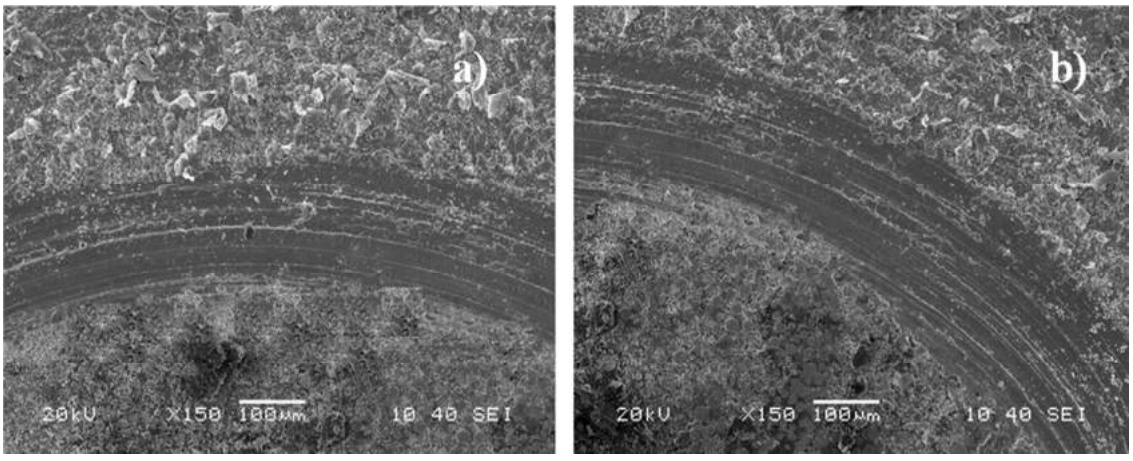

Fig. 11. Micrograph of wear track at (a) 20 N; (b) 30 N load

4. Conclusions:

Following conclusions could be derived from the synthesis of nano ZrO_2 dispersed W based alloy (W-Ni-Mo) by mechanical alloying followed by conventional sintering:

- The mechanical alloying was a potential route to produce nano crystalline alloy powder after 20 h of milling.
- The XRD, SEM, TEM investigation revealed the progressive refinement of crystallite size and decrease in particle size with an increase in lattice strain.
- Sintering of compacted milled powder at 1500°C in Argon atmosphere results in formation of intermetallic compound such as MoNi.
- Dispersion of nano ZrO_2 at grain boundary of W matrix was evident from TEM and EDS analysis of sintered product.
- High Hardness of 4.92 GPa with acceptable wear resistance was achieved due to dispersion strengthening effect of nano ZrO_2 and formation of hard intermetallic.

References:

1. W. F. Smith, *Structure and Properties of Engineering Alloys*, Second Edition, McGraw-Hill, USA, 1993.
2. Anshuman Patra, *Microscopy and analysis*, 26(5) (2012) 14-19.
3. C. Suryanarayana, *Prog. Mater. Sci. 46* (2001) 1-184.
4. D. K. Kolia, G. Agnihotri and R. Purohit, *Procedia Mater. Sci*. 6 (2014) 567 – 589.
5. M. Trazaska, *Int. Jou. Refract. Met. Hard Mater*. 14 (1996) 235.
6. W. E. Gurwell, *Mater Manuf. Process*. 9(6) (1994) 1115-1126.
7. L. Uray, *Int. Jou. Refract. Met. Hard Mater*. 20 (2002) 235.
8. R. Malewar, K.S. Kumar, B.S. Murty, B. Sarma, S.K. Pabi, *J. Mat. Rev.* 22 (2007) 1200-1206.
9. H. Hahn, J. Logas and R.S. Averbach, *J. Mater. Res*. 5 (1990) 609.
10. P. Norajitra, L.V. Boccaccini, E. Diegele, V. Filatov, A. Gervash, R. Giniyatulin, S. Gordeev, V.Heinzel, G. Janeschitz, J. Konys, W. Krauss, R. Kruessmann, S. Malang, I. Mazul, A. Moeslang, C. Petersen, G. Reimann, M. Rieth, G. Rizzi, M. Rumyantsev, R. Ruprecht and V. Slobodtchouk, *J. Nucl. Mater*. 329–333 (2004) 1594-1598.

11. S. Wurster , N. Baluc , M. Battabyal, T. Crosby , J. Du, C. García-Rosales, A. Hasegawa, A. Hoffmann, A. Kimura, H. Kurishita, R.J. Kurtz, H. Li, S. Noh, J. Reiser, J. Riesch, M. Rieth, W. Setyawan , M. Walter, J. H. You and R. Pippan, *J. Nucl. Mater.* 442 (2013) S181- S189.
12. A. Bose, D. M. Si and R. M. German, *Prog. Powder Metall.* 43 (1987) 79-92.
13. Lassner E, Schubert W-D, *Tungsten-properties, chemistry, technology of the element, alloys, and chemical compounds*, Kluwer Academic/Plenum Publishers, New York, 1999, pp. 255-268.
14. Ho J. Ryu and Soon H. Hong, *Mater. Sci. Eng. A*. 363 (2003) 179–184.
15. Y. Kim, K. H. Lee, E. P. Kim, D.I. Cheong and S. H. Hong, *Int. Jou. Refract. Met. Hard Mater.* 27 (2009) 842–846.
16. M. V. Aguirre, A. Martin, J. Y. Pastor , J. LLorca , M. A. Monge and R. Pareja, *J. Nucl. Mater*. 417 (1) (2011) 516–519.
17. B. Cullity, *Elements of X-ray diffraction*, second edition, Addison Wesley, Philippines, 1978, pp. 86-88.
18. G. K. Williamson and W. H. Hall, *Acta Mater*. 1 (1953) 22.
19. Y. H. Zhao, H. W. Sheng, and K. Lu, *Acta Mater.* 49 (2001) 365–375.
20. P. P. Chattopadhayay, P. M.G. Nambissan, S.K. Pabi and I. Manna, *Appl. Surf. Sci*. 182 (2001) 308-312.
21. N. Ozkan and B. J. Briscoe, *J. Eur. Ceram. Soc*. 14 (1994) 143-151.
22. G. Dieter, *Mechanical Metallurgy*, SI Metric Edition, McGraw-Hill, Singapore, 1928, pp. 189–193.
23. K. H. Lin, C. S. Hsu and S.T. Lin, *Int. Jou. Refract. Met. Hard Mater.* 20 (2002) 401–408.
24. M. Nuthalapati, S. K. Karak and A. Basu, *Materials Today: Proceedings*, 2 (2015) 1109 – 1117.
25. P. B. Kemp and R. M. German, *J. less common met*. 175 (1991) 353-368.
26. J. F. Archard, *J. Appl. Phys.* 24 (8) (1953) 981-988.
27. A. Joshi and K.K.S. Mer, *Advanced Materials Manufacturing & Characterization,* Vol 3, Issue 1, (2013) pp. 231-235.